J. Fluid Mech. (1990), *vol.* 218, *pp.* 547–572
Printed in Great Britain

The free-surface signature of unsteady, two-dimensional vortex flows

By DEQUAN YU AND GRÉTAR TRYGGVASON
Department of Mechanical Engineering and Applied Mechanics, The University of Michigan, Ann Arbor, MI 48109, USA

(Received 24 April 1989)

The inviscid interaction of two-dimensional vortex flows with a free surface is studied numerically using a combined vortex/boundary integral technique. The vorticity is modelled as point vortices, vortex sheets and finite area vortex regions. Two problems are studied in considerable detail, the head-on collision of a vortex pair with a free surface and the large-amplitude Kelvin–Helmholtz instability of a submerged shear layer. The interaction is controlled by a Froude number and by the geometric parameters describing the initial vortex configuration. In the large-Froude-number limit, the surface motion follows the vortical flow, but depends only weakly on the actual value of the Froude number. For low Froude numbers, the free surface remains almost flat, and the disturbances caused by the vortical flow decrease rapidly with Froude number.

1. Introduction

The classical approximation in water wave theory is the assumption of irrotational fluid motion. This assumption not only makes the problem much more tractable but the results also account well for observations. While the motion of waves may generally be irrotational, anyone observing a river or ship wakes knows that vortical flow below the surface can generate surface deformations. The surface motions due to the wake left by objects moving on a free surface have recently been the subject of several investigations. The motivation comes to a large extent from observations by remote sensing techniques, which show that in addition to the wave pattern analysed by Kelvin nearly a century ago, ships often leave a narrow mark that persists for several hours. The narrow angle of the mark rules out Kelvin wakes, and although it is not completely clear whether subsurface motion or an alteration in the surface water composition leaves the detectable mark, the cause is likely to be the fluid motion in the wake. The wake consists of rotational, turbulent, high-Reynolds-number flow, and coherent motion could last for a very long time. In an effort to cast some light on the basic mechanisms governing the interaction of vortical flows with a free surface, we present here the surface signature of two simple vortical flows using an inviscid, two-dimensional model.

Sarpkaya (1986) experimentally studied the surface deformation due to the vortex system behind a lifting surface. He identified two types of surface disturbance which he called scars and striations. The scars are surface depressions that appear as a pair behind the body parallel to the direction of motion. These marks appear to be directly related to the trailing vortices and may be two-dimensional in a plane perpendicular to the motion (known as the Trefftz plane to aerodynamicists). The striations, on the other hand, are perpendicular to the direction of motion and have

a more three-dimensional character. Similar experiments have been performed by Hirsa (1990), who also studied the surface deformation due to (essentially) two-dimensional vortex pairs. The two-dimensional vortex pair has also been studied by Sarpkaya, Elnitsky & Leeker (1989). An earlier experiment on the collision of two-dimensional vortex pairs with a free surface was reported by Barker & Crow (1977), but in that work the main emphasis was on the vortex motion, rather than the surface deformations. Bernal & Madnia (1989) investigated the generation of surface waves due to a shear flow by considering a jet below a free surface, and Bernal & Kwon (1989) studied the interaction of a vortex ring with a free surface. Previously, Davies (1966) and Davies & Driscoll (1974) reported on experiments with vortex rings colliding with a free surface; they primarily addressed the rate of surface renewal and the effect of surface contaminants.

Analytical investigations of vortex/free surface interactions are, of course, limited to rather simple situations. Linearized solutions exist for flow over a fixed vortex (e.g. Kochin, Kibel & Roze 1964) and for a vortex moving freely under a free surface (Wehausen & Laitone 1960), while Novikov (1981) discusses the generation of linear waves due to a periodic array of point vortices. For the full nonlinear solutions, it is necessary to turn to numerical techniques. Tryggvason (1988) presents a brief numerical study of surface deformation due to the roll-up of a submerged vortex sheet, and the motion of a point vortex pair toward a free surface has been simulated by Sarpkaya *et al.* (1989) and Telste (1989) using a generalized boundary integral/vortex method developed by Baker, Meiron & Orszag (1982). Marcus (1988) simulated the same problem by a finite difference technique. Willmarth *et al.* (1989) simulated the formation of a vortex pair from an initially flat vortex sheet and compared their calculation with experimental results.

The generation of wake vorticity by ships is reasonably well understood. Saunders (1965) discusses the overall character of the vortices left by a ship, and Lugt (1981), in his excellent survey of vortex motion in ship hydrodynamics (as well as in his more general exposure of vortex motion, 1983), gives several examples. Additional discussions of the various types of vortices shed from ships may be found in Dagan & Tulin (1972), for example.

Considerable progress has been made in numerical simulations of the nonlinear evolution of large-amplitude surface waves during the last decade. Among the first calculations of large-amplitude surface waves by boundary integral methods are Longuet-Higgins & Cokelet's (1976) calculations of the large-amplitude motion of a breaking wave and Salvesen & Kerczek's (1976) calculation of the steady two-dimensional potential flow past a submerged line vortex. These methods have now reached sufficient maturity such that simulations of two-dimensional large-amplitude surface waves are relatively routine; see, for example, Vinje & Brevig (1981), Dold & Peregrine (1986), and Schultz (1987). A general method for flows with arbitrary stratification and an efficient iterative solution technique is presented by Baker *et al.* (1982). For a general review of vortex methods for two-dimensional flows, see Leonard (1980) and Sarpkaya (1989).

In this paper, we study the generation of surface disturbances by a submerged vortical flow and the effect of the free surface on the evolution of the vortical flow. The flow is assumed to be inviscid, incompressible, and two-dimensional, and a combined vortex/boundary integral technique is used. The vorticity is modelled as point vortices, vortex sheets, and finite area vortex regions. Two problems are studied in considerable detail: the head-on collision of a vortex pair with the free surface and the large-amplitude Kelvin–Helmholtz instability of a submerged shear-

layer. Some aspects of both problems have already been studied numerically, see Tryggvason (1988), Marcus (1988), Sarpkaya *et al.* (1989), Telste (1989), and Willmarth *et al.* (1989). But here, we extend these investigations considerably to different vortex models and wider parameter ranges, and we draw some general conclusions. We deal exclusively with free-surface problems, but several of the same phenomena may be observed if the free surface is replaced by a density interface. For one such problem, see Dahm, Scheil & Tryggvason (1989).

The rest of the paper is arranged as follows: §2 discusses the mathematical model, the numerical method, and the relevant dimensionless parameters. The method is a straightforward extension of the method described by Baker *et al.* (1982); hence, we only give a brief description. In §3 we present our results, first for the head-on collision of a vortex pair with the free surface, then for the large-amplitude Kelvin–Helmholtz instability of a shear layer. The large-amplitude stage for several values of the control parameters is shown, and various diagnostic quantities are discussed. Our conclusions appear in §4. A short account of some of the work reported here was presented at the American Physical Society, Division of Fluid Dynamics, Annual Meeting at SUNY, Buffalo (Song, Yu & Tryggvason 1988). A brief discussion of preliminary results can be found in Tryggvason (1988, 1989) and Willmarth *et al.* (1989).

2. Problem formulation and numerical method

The formulation of inviscid, free-surface problems in terms of generalized vortex sheets is well known, so only a brief discussion will be given here. For a fairly complete discussion, refer to Baker *et al.* (1982).

In all our calculations, we use a computational domain of width = 1, with periodic horizontal boundary conditions. The velocity due to a (generalized) vortex sheet of strength γ is then calculated by

$$q^*(s) = u - \mathrm{i}v = \frac{1}{2\mathrm{i}} \int_0^1 \gamma(s) \cot \pi(z(s') - z(s))\, \mathrm{d}s' + q^*_{\mathrm{ext}}, \tag{1}$$

where the integral is over both the free surface and the vortex sheet. Here, s is an arclength coordinate along the sheet, $z(s) = x(s) + \mathrm{i}y(s)$ is the position of an interface point, $q^* = u - \mathrm{i}v$ is the conjugate of its complex velocity, and q^*_{ext} is the velocity due to boundary conditions, or vorticity not confined to a vortex sheet. We generally follow Baker *et al.* (1982) and integrate the dipole sheet strength, $\mu = \phi_1 - \phi_2$ (ϕ_i is the velocity potential in fluid i), in time and find $\gamma = \partial\mu/\partial s$. The evolution equation for μ is found by subtracting the Bernoulli equation on each side of the sheet, which yields

$$\frac{\mathrm{D}\mu}{\mathrm{D}t} = A\left(2\frac{\mathrm{D}\Phi}{\mathrm{D}t} - qq^* + \tfrac{1}{4}\gamma^2 + 2gy + \frac{\sigma}{\rho_2 - \rho_1}\kappa\right). \tag{2}$$

Here, ρ_i is the density in fluid i, g is the acceleration due to gravity, κ is the curvature, σ is the surface tension coefficient, A is the Atwood ratio, $(\rho_1 - \rho_2)/(\rho_1 + \rho_2)$, and Φ is the average of the velocity potential on either side of the integral. To find $\mathrm{d}\Phi/\mathrm{d}t$, we take the Lagrangian time derivative of the real part of Cauchy's integral formula for a periodic domain

$$W(z) = \Phi + \mathrm{i}\Psi = \frac{1}{2\mathrm{i}} \int_0^1 \mu(s') \cot \pi(z' - z)\, \mathrm{d}z', \tag{3}$$

and substitute the result into (2) to obtain an integro-differential equation for the evolution of μ.

To extract the appropriate dimensionless parameters, we cast the above equations into non-dimensional form. We construct our timescale from the characteristic length of the rotational flow, L, and the characteristic velocity, Γ/L, where Γ is a circulation describing the total strength of the vorticity field. A timescale is then given by L^2/Γ. With the non-dimensional variables, denoted by a tilde, defined as

$$(x, y) = L(\tilde{x}, \tilde{y}), \quad t = L^2/\Gamma\tilde{t}, \quad (\bar{q}, \gamma) = \Gamma/L(\tilde{q}, \tilde{\gamma}), \quad (\Phi, \mu) = \Gamma(\tilde{\Phi}, \tilde{\mu}), \tag{4}$$

the non-dimensional form of the equation for the vortex sheet strength becomes (dropping the tilde)

$$\frac{\mathrm{D}\mu}{\mathrm{D}t} = A\left(2\frac{\mathrm{D}\Phi}{\mathrm{D}t} - qq^* + \tfrac{1}{4}\gamma^2 + 2\frac{1}{Fr^2}y + \frac{1}{We}\kappa\right), \tag{5}$$

where $Fr = (\Gamma^2/gL^3)^{\frac{1}{2}}$ is a Froude number, and $We = \Delta\rho\Gamma^2/\sigma L$ is a Weber number.

The non-dimensional groups specifying our problem are therefore the Froude number, Fr; the Weber number, We; and the geometric parameters describing the initial condition. The Atwood number, A, is always equal to unity for the free-surface case studied here, and in most of our calculations we assume an infinite Weber number. Our scaling, equation (4), essentially ignores the presence of the free surface, and the same non-dimensional time therefore means that the vortex sheet evolution has progressed equally far, independent of Fr. Obviously, this is not the only possible scaling. We could also base our non-dimensionalization solely on the free surface, in which case the basic non-dimensional parameter would be a non-dimensional vortex strength equivalent to the Froude number. The timescale would, however, be different. We feel that the current 'vortex scaling' is the reasonable one, since the vortical flow is what drives the motion. We should note that in Tryggvason (1988), as well as in Dahm *et al.* (1989), the basic non-dimensional parameter is written as $R = gL^3/\Gamma^2 = 1/Fr^2$. Clearly, there is a one-to-one correspondence with the current notation.

In those calculations where the vorticity is modelled as vortex sheets, we represent the sheets by vortex blobs to prevent the formation of a singularity and to eliminate short-wave instabilities. Krasny (1986) shows that in contrast to simulations that do not employ any regularization, vortex-blob methods, for any finite blob size, produce smooth, well-behaved vortex sheets for sufficiently accurate calculations. The evolution in the vortex centre will depend on the blob size, but the effect on the large-scale structure is minimal. Most of our results have been checked for the influence of the blob size, and the results presented are insensitive to the exact value of the blob. In the interest of brevity, these checks are not included in this paper, and can be found in Yu (1990). For further discussions of the vortex blob regularization, the reader is referred to Krasny (1986, 1988).

Occasionally, a saw-tooth instability on the free surface appears in our computations. This instability is common in boundary integral calculations and can generally be controlled by a slight smoothing, see Longuet-Higgins & Cokelet (1976). In those runs where such filtering is required, it is employed rarely at the beginning of the calculation and more frequently later. We have found that the dipole formulation, described above, is more robust than the vorticity formulation, which was used for the calculations in Tryggvason (1988, 1989). The simulations generally had to be terminated when the free surface formed a sharp corner and difficulties in

obtaining rapid convergence were experienced. Although we expect such segments of high curvature to indicate a region where our inviscid model no longer accurately reflects the underlying physical problem (small-scale phenomena such as viscosity and surface tension have been ignored), we should note that there is not a direct relation to loss of convergence and, say, wave breaking. Occasional redistribution of the free-surface points is used in some of our runs, and time integration is done by STEP from Shampine & Gordon (1965).

In several of our calculations we take the vorticity to be patches, or strips, of uniform vorticity (called Finite Area Vortex Regions (FAVRs) by Zabusky, Hughes & Roberts 1979). Because of some mathematical difficulties in calculating $D\Phi/Dt$ in (2), we integrate the vortex sheet strength directly, as done by Tryggvason (1988), instead of using the dipole formulation as in the other calculations. The evolution equation for the vortex sheet strength of the free surface is obtained either by differentiation of (2) or by subtracting the tangential component of the Euler equations on either side of the interface. This equation contains $d\bar{U}/dt$, which is given by the Lagrangian time derivative of the Biot–Savat law and the velocity contribution from the FAVRs:

$$q_{\text{ext}}(z) = u(z) + iv(z) = \frac{\omega}{2\pi}\oint (\log|\sin\pi(z-z')|)\,dz'. \tag{6}$$

Here, the integral is over the boundary of the region containing a uniform vorticity, ω.

3. Results and discussion

3.1. *Vortex pair approaching a free surface*

Motivated by the experiments of Sarpkaya (1986) and Hirsa (1990), we consider a vortex sheet with a vortex sheet strength corresponding to a wing with elliptic loading and a negative angle of attack; the vortex sheet lies at a relatively small initial depth below the free surface (1.25 non-dimensional units). This vortex sheet rolls up into a vortex pair that propagates upward. The length in the definition of the Froude number is taken as the separation that the vortices would have in the absence of a free surface, estimated by assuming that the sheet will become a pair of point vortices. The free surface and the vortex sheet are discretized by 200 points each. To regularize the vortex sheet, we use the algebraic vortex blob employed by Krasny (1986) to represent the sheet; the vortex blob radius, δ, is relatively large and equal to 0.5 times the separation between the vortices. Several of our vortex sheet runs have been repeated with different blob radii, as well as different numbers of computational points, to confirm that the effect of finite δ is minimal and confined to the vortex cores, see Yu (1990).

Figure 1 shows the evolution of the vortex sheet and the free surface for three different Froude numbers. The first sequence, (*a*), is for a strong Froude number of 11.2; the second one, (*b*), is for an intermediate Froude number, 3.54; and the last one, (*c*) is for a low value of 1.58. The vortex blobs representing the vortex sheet are connected by straight lines in these figures, except where the sheet has undergone large stretching and the points are left unconnected. The Froude numbers in figure 1 have been selected because the evolution in each case is representative for a range of Froude numbers. Strong vortices, as in (*a*), are little affected by the surface during the time shown here. As the vortex pair approaches the surface, it pushes the surface

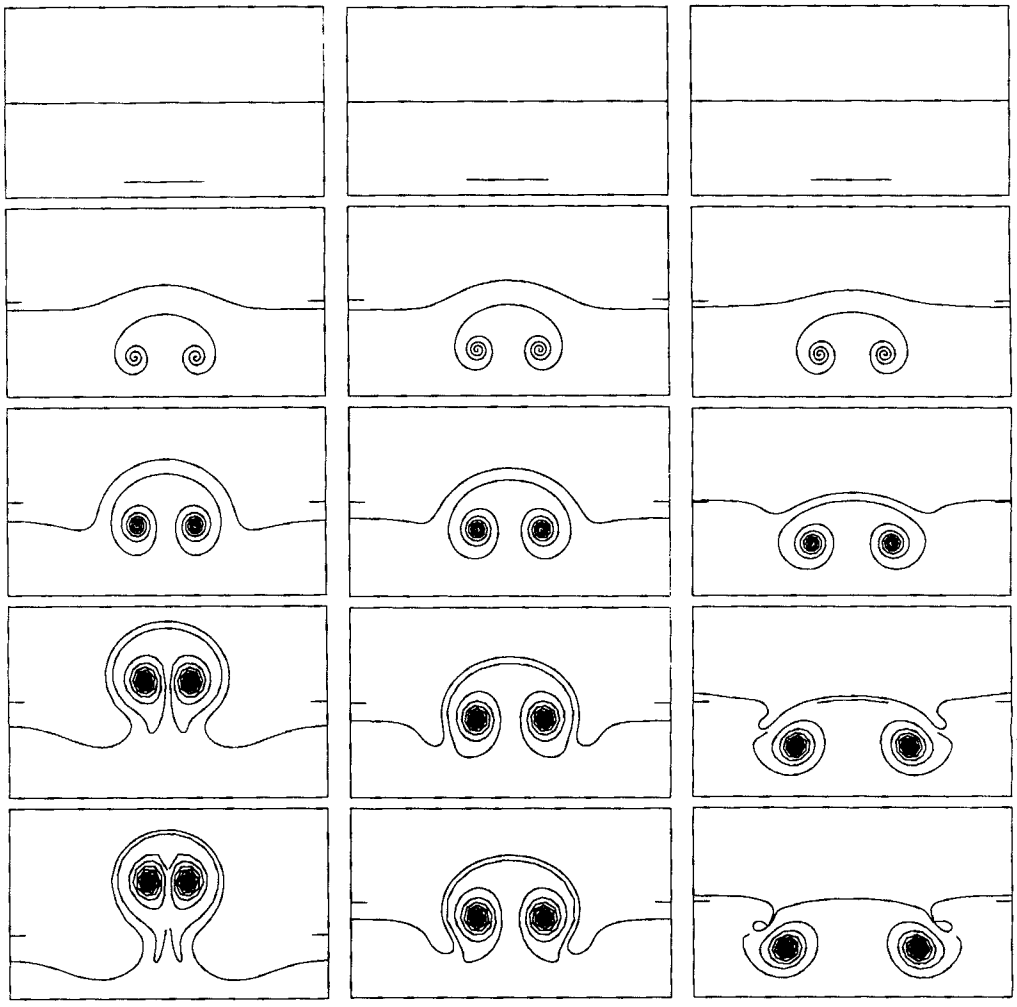

FIGURE 1. The collision of a vortex pair, formed from a vortex sheet, with a free surface. The initial depth $d/L = 1.25$. The non-dimensional times are 0, 3.0, 6.0, 9.0 and 10.5. (*a*) $Fr = 11.2$; (*b*) $Fr = 3.54$; (*c*) $Fr = 1.58$.

upward, and subsequently, the pair propagates out of the main fluid region, carrying a considerable amount of fluid with it. At the same time, since the length of the period is finite, the level of the fluid left behind drops to conserve mass. The speed of the vortex pair is minimally affected by the presence of the free surface. Baroclinically generated vorticity at the free surface obviously opposes the vortex motion, but at the same time pushes them slightly together, compensating for the effect of the surface. Shortly after the last stage shown, the iterative procedure failed to converge, and the calculations were terminated. In (*b*), the initial surface deformation is similar to the high-Froude-number case, but after the initial bump forms, the vortices start to move apart and the rise of the fluid stops. At the same time, the interface is rapidly pulled down in front of the vortices. For the low Froude number in (*c*), the surface deformation is reduced, and the vortices move outward

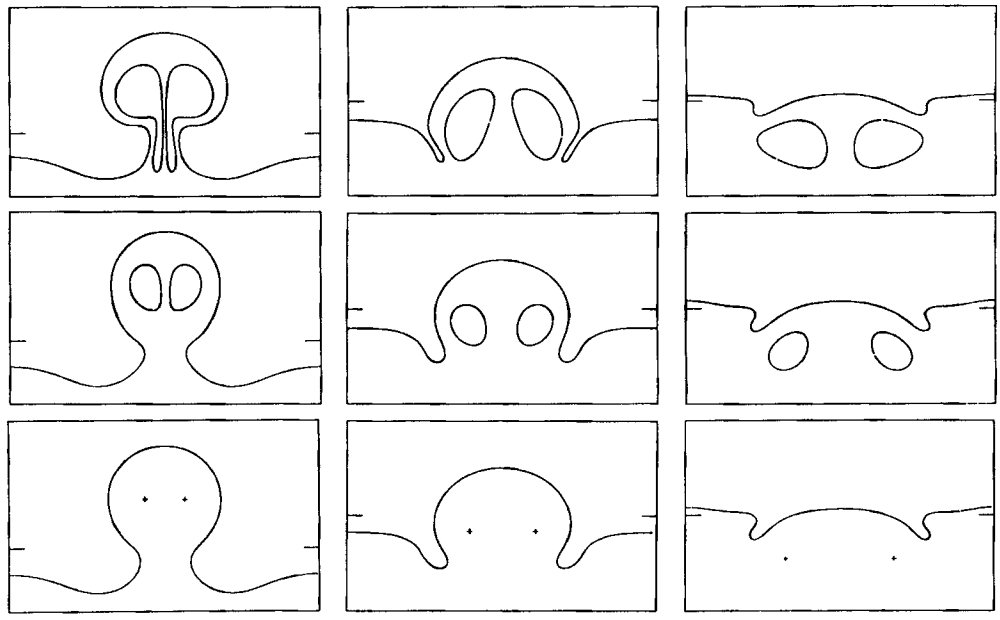

FIGURE 2. The late-time solution for the collision of a finite area vortex pair and a point vortex pair with a free surface. The initial depth $d/L = 1.25$. The initial diameter of vortex patch, t/L, is 0.45 in the top row, 0.3 in the middle one and the bottom row contains the point vortex results. (*a*) $Fr = 11.2$; (*b*) $Fr = 3.54$; (*c*) $Fr = 1.58$. The non-dimensional time is 10.0 in (*a*) and (*b*), and 9.0 in (*c*).

much like the surface was a solid wall. A depression forms in front of the vortices and eventually leads to overturning and entrainment of the top fluid.

As is well known, vortex blobs, as we have used to represent the sheet are not exact solutions of the Euler equations. Furthermore, even though the vortex blob representation converges to a vortex sheet at early time (Caflisch & Lowengrub 1989), it is not known whether the vortex blob results converge at large time. To investigate the effect of different core structures, as well as to present results that are not subject to the above-stated deficiency (of not being exact solutions of the Euler equations), we have repeated the calculations with the vortices modelled as vortex patches, or finite area vortex regions (FAVRs). There is now an additional geometric lengthscale, namely, the size of the vortex patch. In addition, we have modelled the vorticity as point vortices, as done by Telste (1989) and Sarpkaya *et al.* (1989). In figure 2, we show the results at late time for three different Froude numbers: 11.2 in the left column, 3.54 in the middle one, and 1.58 in the right column (the same as in figure 1) for runs with two different patch radii and point vortices. The time is 10.5 for the larger Froude numbers, and 9.0 for the lowest Froude number. In the top row the diameter of the patch is 0.45 times the separation of the centres, and in the middle row the diameter is 0.3 times the separation. The results for the point vortices are in the bottom row. The initial depth is 1.25 times the separation, the free surface is discretized by 300 computational elements, and the bounding curve of each vortex patch is discretized by 100 elements.

Generally, these results correlate well with the vortex sheet calculations in figure 1. For the highest Froude number, the fluid blob carried with the large patch is slightly wider, but lower, than that for the patch with a smaller diameter and for the

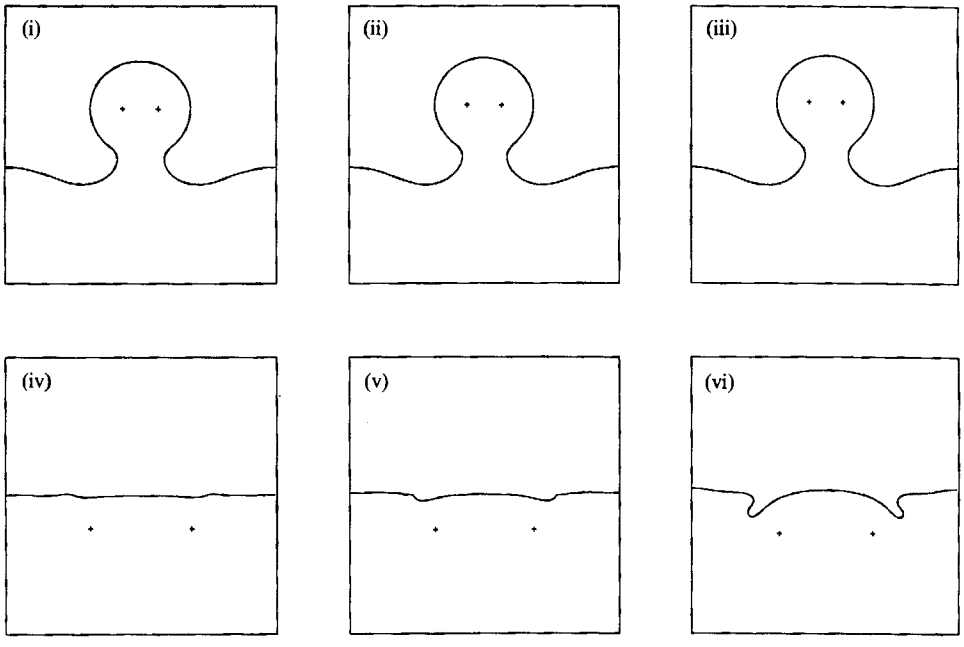

FIGURE 3. The late-time solution for the collision of a point vortex pair with a free surface. (i) $Fr = 11.2$; (ii) $Fr = 15.8$; (iii) $Fr = 22.4$; (iv) $Fr = 0.50$; (v) $Fr = 0.79$; (vi) $Fr = 1.58$. The non-dimensional time is 10.0 in (i), (ii), and (iii) and 9.0 in (iv), (v), and (vi). In all cases, $d/L = 1.25$.

point-vortex case. This could be partly due to some of the vorticity actually being left behind in the neck that connects the fluid blob with the rest of the fluid. For the intermediate Froude number, there is also very little difference between the small-patch and the point vortex results, but the spike of top fluid pulled down at the outer edges of the vortices is thinner for the large patch. In the small-Froude-number case, again, the difference between the middle and the right column is small, but for the large patch a slight reduction in the surface amplitude is apparent. For all Fr, there is almost an exact agreement between the point-vortex case, the small-patch case, and the vortex sheet calculations in figure 1. This, of course, does not come as a surprise, since the elliptic vortex sheet distribution leads to a rather concentrated vorticity distribution, once roll-up is completed.

The results in figures 1 and 2 obviously show that the surface deformation depends strongly on the Froude number. To assess the dependency in more detail, we have run several cases for Froude numbers both larger and smaller than those shown in the previous figures; in most cases we use point vortices to model the vortical flow. These runs show that the evolution can be classified two ways: (i) the large-Froude-number case, where the vortices propagate through the free surfaces, as in figures 1(*a*) and 2(*a*) and (ii) the small-Froude-number case, where the free surface acts like a rigid boundary, as in figures 1(*c*) and 2(*c*). The transition from one type of motion to another takes place over a relatively small range of Froude numbers, and once these limits are reached the motion is relatively weakly dependent on the actual value of the Froude number.

In figure 3, we have plotted the solutions at late time for several 'high' Froude numbers and several 'low' Froude numbers. Frames (i), (ii), and (iii) are at time 10 for Froude numbers 11.2 (as in figures 1*a* and 2*a*), 15.8 and 22.4, respectively. It is

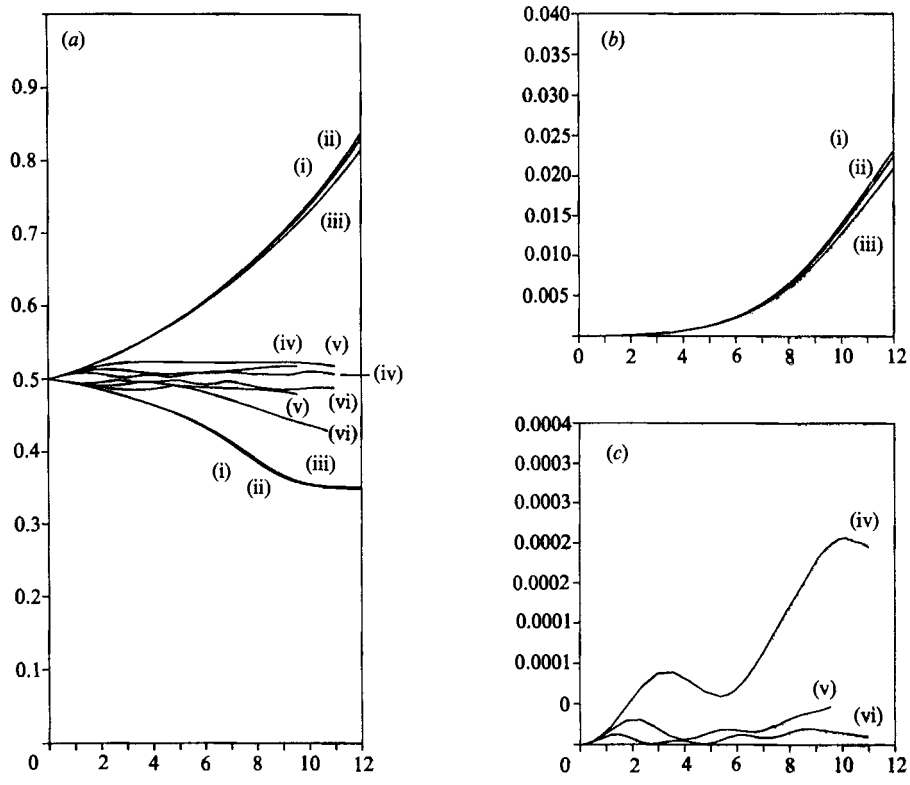

FIGURE 4. (*a*) The maximum and minimum free-surface elevations for the runs in figure 3 versus time. (*b*) The potential energy for the 'high' Froude numbers (11.2, 15.8 and 22.4) versus time. (*c*) The potential energy for the 'low' Froude numbers (1.58, 0.79 and 0.5) versus time. The profiles correspond to the frames in figure 3.

obvious that doubling the Froude number has rather minor effects. Frames (iv), (v), and (vi) are for Froude numbers 0.5, 0.79 and 1.58 (as in figures 1*c* and 2*c*) at time 9.0. Although the overall shape of the surface deformation is similar, some changes occur as the Froude number decreases; in addition, the amplitude becomes smaller. A closer inspection (substantiated by additional runs) shows that the position of the maximum surface depression is closer to the vortex for the lower Froude number, so that in the limit of zero Froude number we would expect the depression to coincide with the vortex position. This is in agreement with what we observe in the next section and with Novikov's (1981) analytical, small-amplitude prediction for a vortex moving steadily below a free surface.

To demonstrate some of our conclusions more clearly, in figure 4 we plot both the maximum and minimum amplitudes, as well as the potential energy versus time, for the runs in figure 3. The maximum and minimum surface elevations are shown in figure 4(*a*). The maximum surface elevation for the large Froude numbers increases continuously, while for the lower Froude numbers the elevation reaches a maximum at a much lower level and changes only slightly during the last part of the run. Notice in particular the insensitivity of the high-Froude-number cases to the Froude number. We should note that the significant drop in minimum elevation for the high-Froude-number case is mostly due to the finite extent of our computational box. For larger boxes, the removal of a fluid blob from the main fluid region results in much

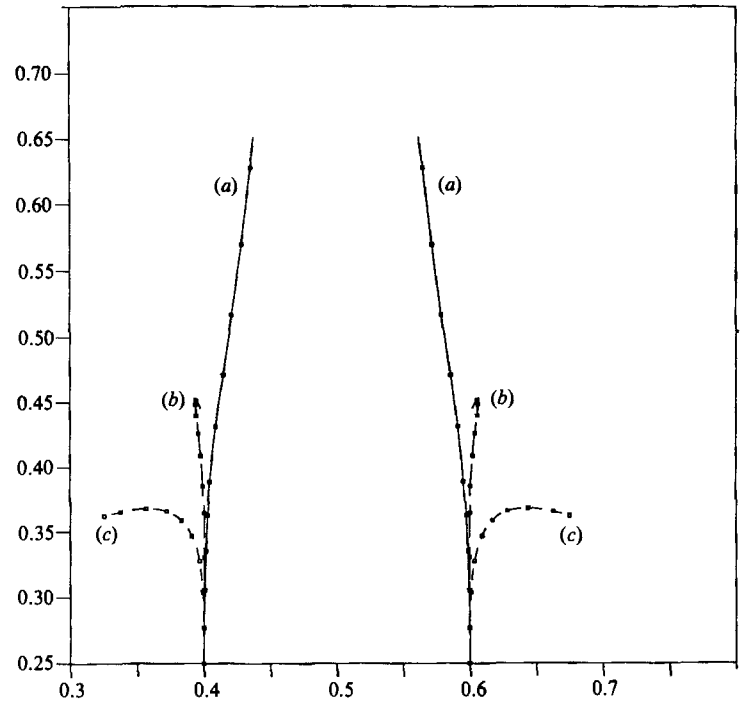

FIGURE 5. The path of the point vortices for (*a*) $Fr = 11.2$; (*b*) $Fr = 3.54$; (*c*) $Fr = 1.58$ (the bottom row in figure 2). The distance between the dots on each line marks a time interval of 1.0.

smaller changes in the level of the fluid left behind. The plots of potential energy versus time, in figures 4(*b*) and 4(*c*), reflect the amplitude of the surface motion of the cases plotted in figure 4(*a*). (Note that the scale is different for the graphs in figures 4(*b*) and 4(*c*).) For the large Froude numbers, the potential energy increases continuously, reaching an approximately constant growth rate at the end of the run. In the case of small Froude numbers, the growth is oscillatory and considerably smaller. The oscillations in this case are presumably partly due to transients set up by the impulsive generation of the rather shallow point vortices.

To show the effect of the surface on the vortical motion, in figure 5 we plot the path of the vortices for Froude numbers 11.2, 3.54 and 1.58. Dots on the path at regular time intervals equal to 1.0 give an indication of the speed. In the large Froude number case, where the vortices penetrate the interface, the paths converge, and the reduction in distance between them more than compensates for the reaction from the surface, so that their speed actually increases. The vortices in the low-Froude-number case move outward, as if the surface was a solid wall. However, their path differs slightly from the solid-wall case, owing to the surface deformations, and a small rebounding is seen. The intermediate path first diverges slightly and then turns inward. These calculations could not be continued past the point shown, but we expect that the vortex would eventually complete a loop and move outward. Such behaviour is observed for vortices encountering weak density interfaces, see Dahm *et al.* (1989).

We have repeated many of our calculations with a higher number of computational elements and monitored the energy balance to assess the accuracy of our methods. For the range of computational elements used here, doubling the number of elements

has virtually no effect. The accuracy of our calculations is also reflected by the almost total conservation of energy, which is generally a rather sensitive measure of the quality of a solution. In addition, we have compared our calculations to those reported by Telste (1989). He uses a similar method but applies a damping layer at the edge of his computational domain to model an infinite horizontal length. His results for Froude numbers 7.07, 2.24 and 0.5 and an initial vortex depth five times the vortex separation agree well with what would be expected from the simulations presented here. Telste also found energy to be well conserved for the time he simulated. The influence of the relatively small computational box has also been checked by repeating the calculations in both a narrower and a wider box. Although these tests show that the box width has some influence on the evolution (for example, the wider the box, the less the level of the lower fluid drops for large Froude numbers), the essential interaction mechanism remains unchanged for all but the narrowest boxes. We therefore firmly believe that the results obtained here for a finite horizontal fluid domain are representative for infinite domains as well and that our conclusions from these studies apply equally to that case. For a more detailed discussion of these tests, see Yu (1990).

The inviscid models studied here are all scale invariant and, thus, are applicable to a wide range of physical lengthscales. In the wake of a ship, for example, we would generally expect that while the results for small Froude numbers might describe the largest scales of the flow, the high-Froude-number results, where the vortical flow leads to rather dramatic 'splashes', would be more applicable to the small-scale turbulent motion (such as the generation of 'white water wakes' due to propellers). At small scales, however, the scale invariance of the inviscid model is broken by either viscosity or surface tension. While viscosity is not easily incorporated into our model, surface tension is. The effect of surface tension on the free-surface deformations due to the collision of a strong point vortex pair is shown in figure 6; here we compare the late time stage ($t = 9.8$) of three simulations with a Froude number of 11.2 for $We = 1.0$, $We = 3.0$, and an infinite Weber number. The increased surface tension reduces the growth of the surface deformation and leads to a larger separation of the vortices. For even smaller Weber numbers, the surface deformation is largely inhibited, but several short waves appear on the surface. These waves could be capillary waves, but we have not ruled out numerical difficulties as a cause. Large surface tension results in a very stiff system, and minute timesteps are necessary.

3.2. *Shear layer under a free surface*

We now consider a free surface with flow parallel to the surface. At depth d there is a shear layer such that the velocity changes abruptly. Our frame of reference moves with the average of the velocity above and below the shear layer, so that a vortex generated by a large-amplitude Kelvin–Helmholtz instability would be stationary if the free surface was absent. The period length, L, is taken as a lengthscale, and the evolution is governed by the Froude number, the relative depth of the shear layer, d/L, and, possibly, the internal structure of the layer.

The shear layer is first modelled as a vortex sheet across which there is a discontinuous change in the tangential velocity. Figure 7 shows the vortex sheet and free surface for several times. Here, $Fr = 0.5$ and $d/L = 0.2$. The free surface is represented by 200 computational elements, and the vortex sheet by 200 vortex blobs; we use $\delta = 0.1$ in this case. The free surface is initially flat, but the vortex sheet is perturbed slightly by a single wave. As the vortex sheet rolls up, the induced velocity causes a depression in the free surface that remains relatively stationary

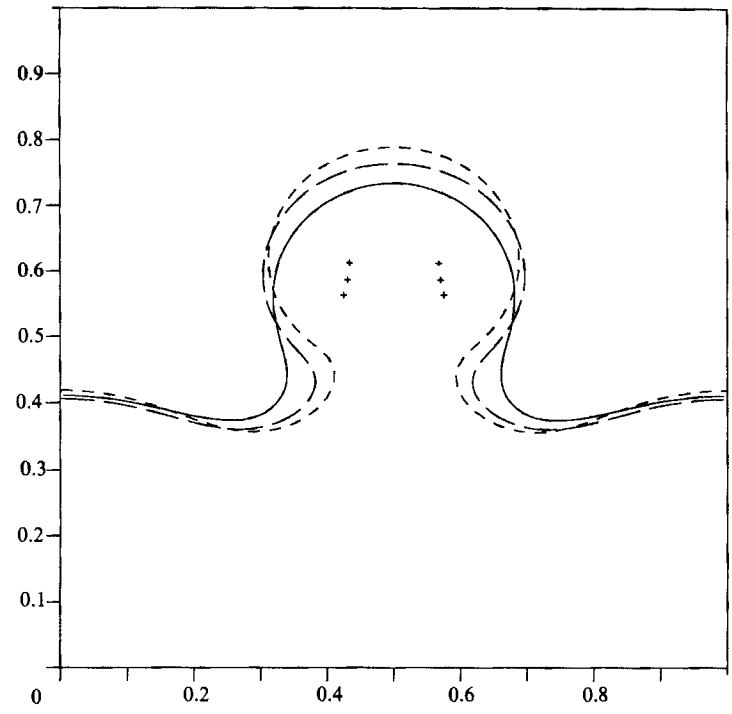

FIGURE 6. A comparison of the evolution of a free surface for different surface tension and $Fr = 11.2$. Non-dimensional time is 9.8. ——, $We = 1.0$; — — —, $We = 3.0$; – – –, $We = \infty$.

slightly to the front (or left) of the vortex. As the amplitude grows, the trough becomes steeper on its left side and eventually turns over, suggesting a breaking wave. Note that for this particular selection of governing parameters, the surface mark is a single, relatively localized depression in the free surface.

To investigate the effect of the two control parameters, the Froude number and the relative depth, we have made a large number of simulations. The results from some of these runs are presented in figure 8, which shows the free-surface profile for various Froude numbers, from 2.83 to 0.177, at a relative depth of $d/L = 0.2$ in the first column, $d/L = 0.3$ in the middle one, and $d/L = 0.4$ in the last column. The time is 1.25 for the first column, 1.6 for the second, and 2.0 for the third; for the highest Froude numbers we have also plotted the surface at a later time, which is noted in the figure where relevant. Some of the profiles have been amplified several times, as indicated.

Several changes occur as the governing parameters are varied. First of all, the overall magnitude of the surface deformation decreases both with decreasing Froude number and increasing depth. For high Froude numbers and shallow vortex sheets the free surface is pulled down into the fluid, but for deeper vortex sheets (and high Froude numbers) the depression is pushed left to the boundary of the periodic domain, and no entrainment occurs. At the earlier times, the results for highest Froude numbers are relatively independent of the Froude numbers for a given d/L, with the possible exception of the deepest vortex sheet case where the times shown are relatively large. As the Froude number is decreased, the maximum depression moves toward the centre in all cases and the free surface becomes more localized. The left-hand side of the depression becomes steeper and appears to lead to a breaking

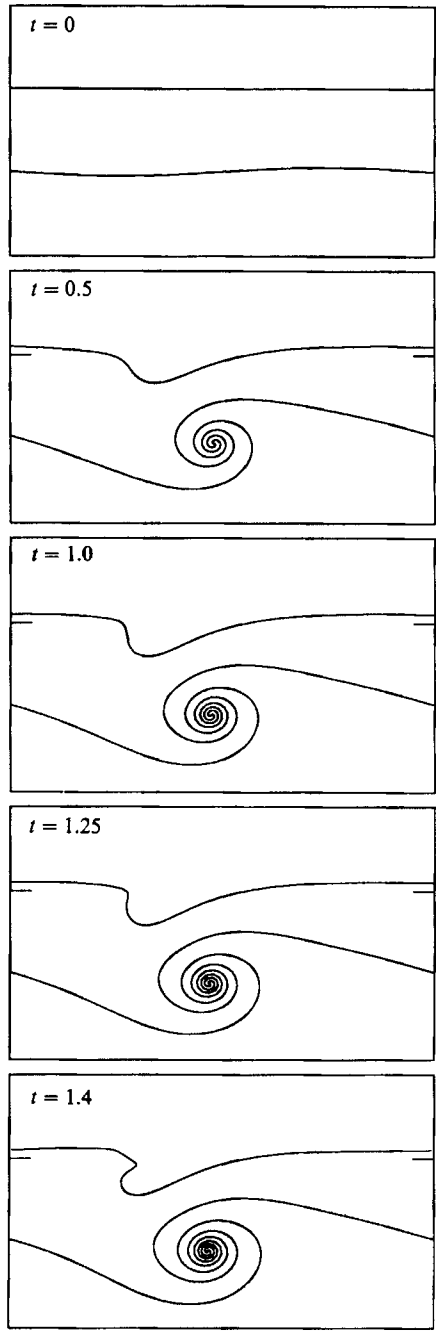

FIGURE 7. The evolution of a free surface and a submerged vortex sheet for $Fr = 0.5$, $d/L = 0.2$. Here $\delta = 0.1$.

wave for $Fr = 0.5$ and all depths, and also for lower Froude numbers, when the vortex sheet is shallow. As the Froude number is reduced further, the steepening of the left-hand side of the trough leads to a generation of smaller waves instead of a single breaking wave. For the lowest Froude numbers, particularly in the deep case, the overall appearance of the surface deformation is similar, but the amplitude

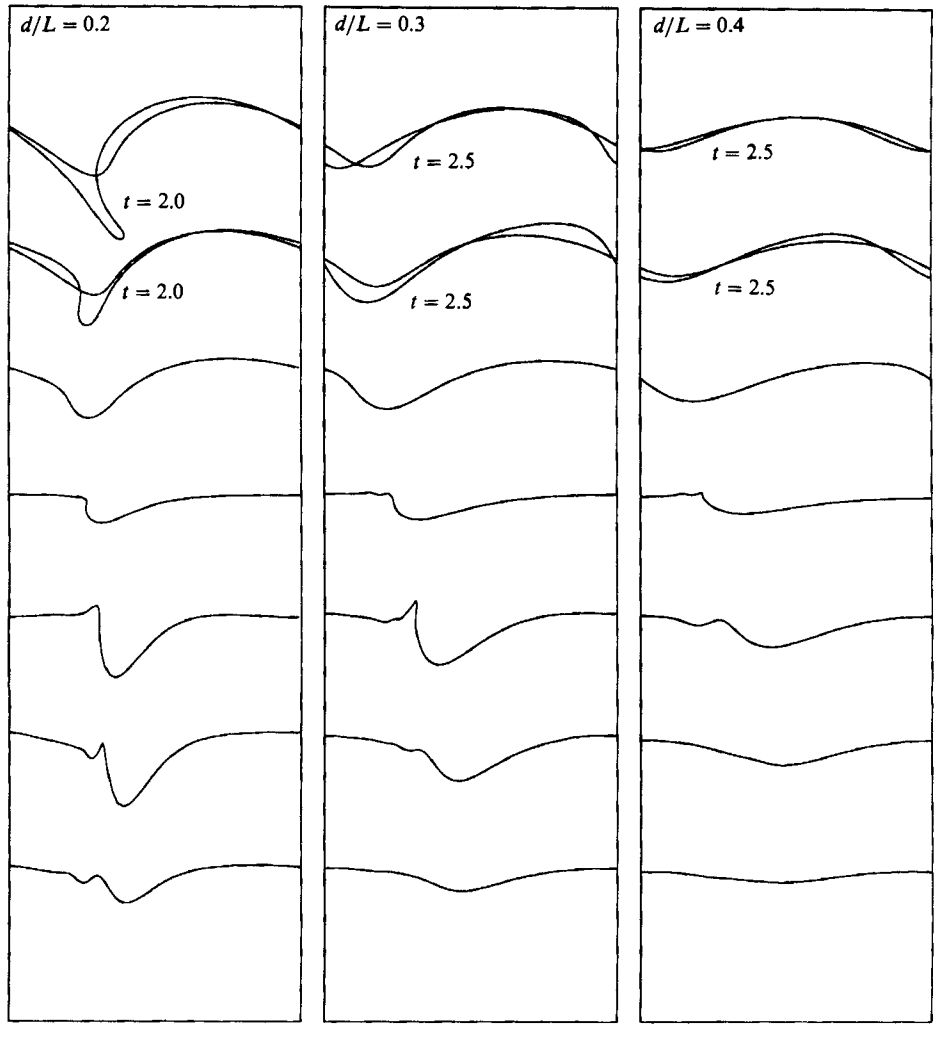

FIGURE 8. A large-amplitude stage for various values of the non-dimensional parameters. From top to bottom, $Fr = 2.83, 1.41, 1.0, 0.5, 0.354, 0.25, 0.177$. The non-dimensional times are approximately 1.25 for $d/L = 0.2$, 1.60 for $d/L = 0.3$ and 2.0 for $d/L = 0.4$.

decreases with Froude number. When the vortex sheet is very weak and deep, the main surface mark is a single shallow depression directly above the vortex.

In order to demonstrate better some of the characteristics of the evolution, in figure 9 we plot some quantitative information for the runs in figure 8. For clarity, the figure is divided into three columns, as figure 8, according to the value of d/L. The numbers in each column correspond to the profiles in figure 8, counted from top to bottom. The maximum and minimum surface elevations are shown in figure 9(*a*). The trend observed in figure 8, that the magnitude of the disturbance decreases with decreasing Froude number and increasing depth, is clear from the plot. Notice, in particular, that the results for large Froude numbers (profiles 1, 2, and 3) are all in good agreement with each other for a relatively long time (up to at least $t = 1.0$), although eventually they diverge. For high Froude numbers, and the shallower sheets, the maximum amplitude eventually reaches a maximum, while the depth

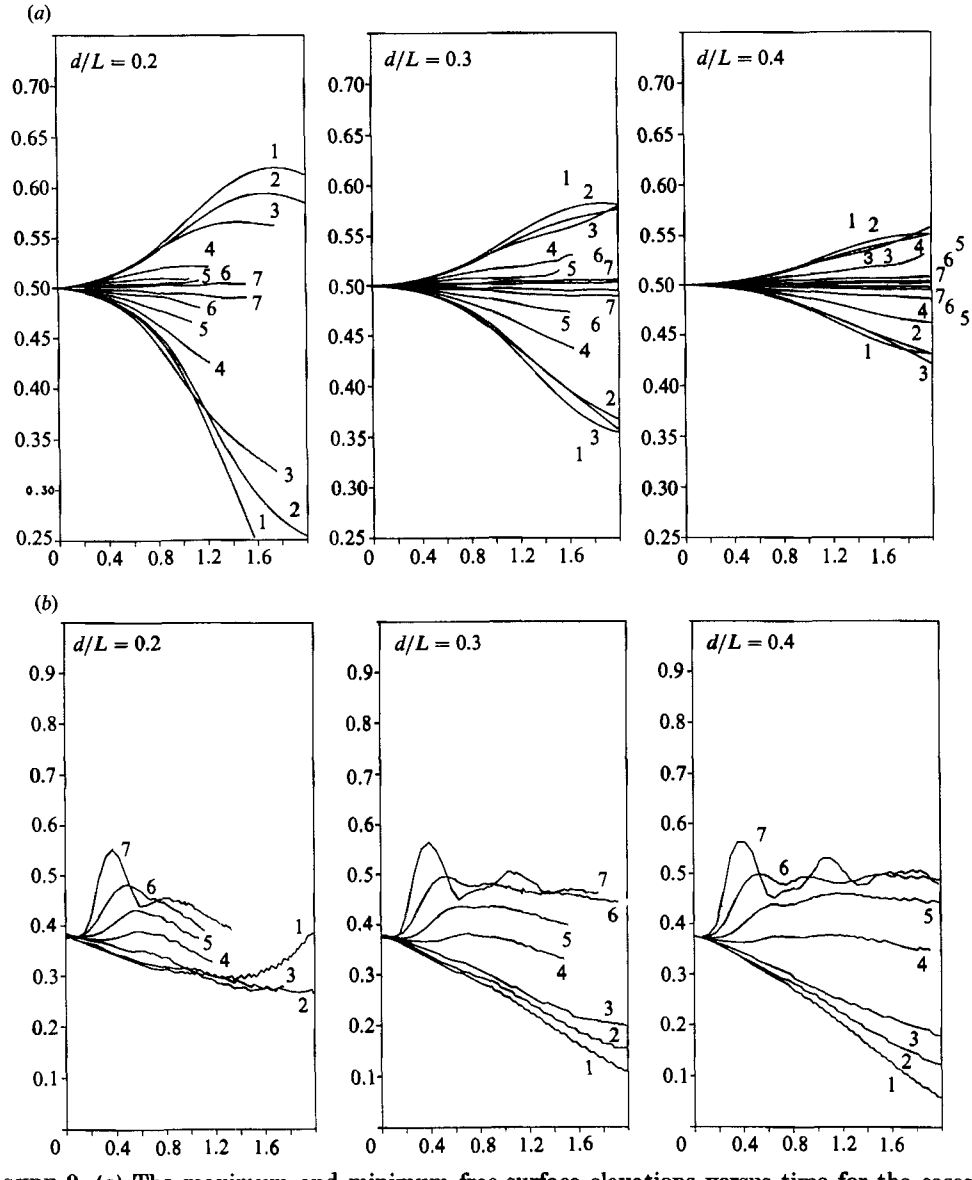

FIGURE 9. (*a*) The maximum and minimum free-surface elevations versus time for the cases in figure 8. (*b*) The horizontal location of the maximum free-surface depth versus time for the runs in figure 8. In each frame the numbers correspond to the profiles in figure 8 (counted from top to bottom).

continues to increase for the duration of the calculations, suggesting entrainment of air into the water. For the lower Froude numbers (profiles 4–7), the growth of the surface disturbance is much slower and shows a continuous dependency on the Froude number.

In figure 9(*b*), the horizontal location of the maximum depth of the free surface is plotted. Initially, when the amplitude is still infinitesimal, the depression is slightly to the left of the vortex (which is at 0.5) for all cases. At high Froude numbers, this depression moves further to the left, but for lower Froude numbers it moves to the right, closer to the vortex. For shallow vortices, this motion to the right eventually

reverses, and the depression again moves away from the vortex, but for deeper vortices the depression seems to stabilize close to the vortex (right above the vortex in the case of the lowest Froude number). Notice that, up to about $t = 0.75$, the motion, while strongly dependent on the Froude number, is virtually independent of the depth. Also, for a fixed time, there is a much greater difference in the location of the depression for the deep vortices than for the shallow ones. In some sense, the shallow vortices appear to attract the depression to a fixed location independent of the Froude number. The slight oscillations for low Froude numbers and deep vortex sheets are indicative of the generation of shorter, smaller waves. Again, note that the results for large Froude numbers are essentially identical until at a relatively late time.

Based on figures 8 and 9 the results may be summarized as follows: for very strong vortex sheets, the free surface moves essentially as a material line for a long time compared with the time it takes the instability of the vortex sheet to develop. Depending on the value of d/L, two things can happen. If the relative depth is small, so the surface passes through the region of fluid that is trapped around the vortex (for a periodic row of point vortices this depth is about 0.28 times the separation of the vortices), the vortex will pull the surface down and the lighter (zero density) top fluid will be entrained in the bottom fluid. If the free surface is above the streamline enclosing the trapped fluid, the vortex cannot pull the fluid down, and the surface will simply move until it coincides with a curved streamline above the vortex. The maximum elevation will then be directly above the vortex. As the Froude number decreases, the ability of the vortex flow to deform the surface is reduced. This manifests itself first in the formation of a breaking wave, and then, at lower Froude numbers, in the generation of shorter waves. For deep vortex sheets, the generation of short waves seems to take longer as the Froude number is reduced, and it is likely that the limiting case at $Fr \to 0$ is simply a slight stationary depression above the vortex.

Although the effect of the size of the vortex blob is minimal in most of the cases considered (see Yu 1990), the solution with a finite blob is not exactly a solution to the Euler equation, as mentioned before; furthermore, there is no direct relation between the size of the blob and a physical stabilization mechanism such as a finite thickness. To investigate the effect of a finite thickness, we have repeated several of the simulations in figure 8 using a layer of uniform vorticity, i.e. finite area vortex regions (FAVRs), to model the shear layer. (For a study of roll-up of a layer of uniform vorticity in the absence of a free surface see e.g. Pozrikidis & Higdon 1985). Figure 10 shows the solution at large time for several Froude numbers and depths. The top two frames are for $Fr = 1.0$ and $d/L = 0.2$ (the depth is to the middle of the layer), the middle two frames for $Fr = 0.5$ and $d/L = 0.3$, and the bottom frames for $Fr = 0.354$ and $d/L = 0.4$. The frames on the left-hand side are for an initial layer thickness $t/L = 0.1$, and the ones on the right-hand side for $t/L = 0.15$. The times all differ, but the right-hand column has the larger times (the exact times are indicated in the figure). While the evolution is similar to the corresponding vortex sheet run (figure 8), the deformation rate is smaller for the finite layer. We note that vorticity layers of finite thickness have a most unstable wavelength (at $t/L \approx 0.127$) as opposed to vortex sheets, which are most unstable for shorter disturbance lengths. Since the thickness in our simulations is close to this value, the slower growth of the disturbances in figure 10 is presumably a more realistic prediction for a real shear layer than the vortex sheet simulations in figure 8.

In figure 11, the maximum and minimum amplitudes are plotted in the left-hand

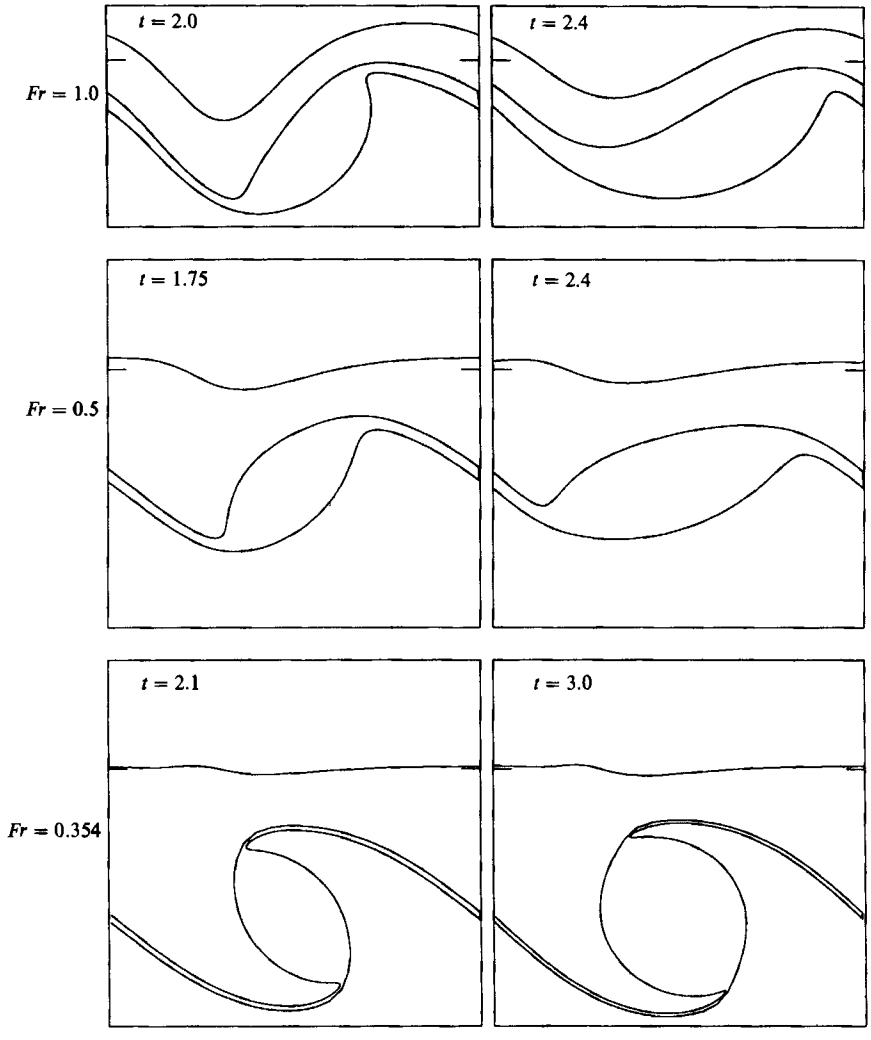

FIGURE 10. The large-amplitude stage of a free surface and a shear layer of the finite thickness. Top row: $d/L = 0.2, Fr = 1.0$; middle row: $d/L = 0.3, Fr = 0.5$; bottom row: $d/L = 0.4, Fr = 0.354$. In the left-hand column the initial vortex-layer thickness, t/L, is 0.1; in the right-hand one t/L is 0.15.

column versus time and compared to the corresponding vortex sheet runs. The amplitude growth obviously depends on the thickness, with the thinner layers in reasonable agreement with the vortex sheet calculations for the lower Froude numbers. The horizontal position of the maximum depth, plotted in the right column in figure 11, is also in reasonable agreement for the shear layer and the thinner vortex layer for $Fr = 1.0, 0.5$ and 0.354 (i.e. motion to the left for shallow layers, and to the right for deep layers). The general conclusion is that we may expect some dependency on the internal structure of the shear layer, but for thinner layers, in particular for low Froude numbers and deep vortex sheets, the surface signature will be closer to the one generated by the vortex sheet model.

During the initial stage in all cases, and for a long time when the vortex sheet is deep and weak, the surface deformation is quite small. It is therefore natural to ask whether linear analysis is applicable under these circumstances. Unfortunately, it is

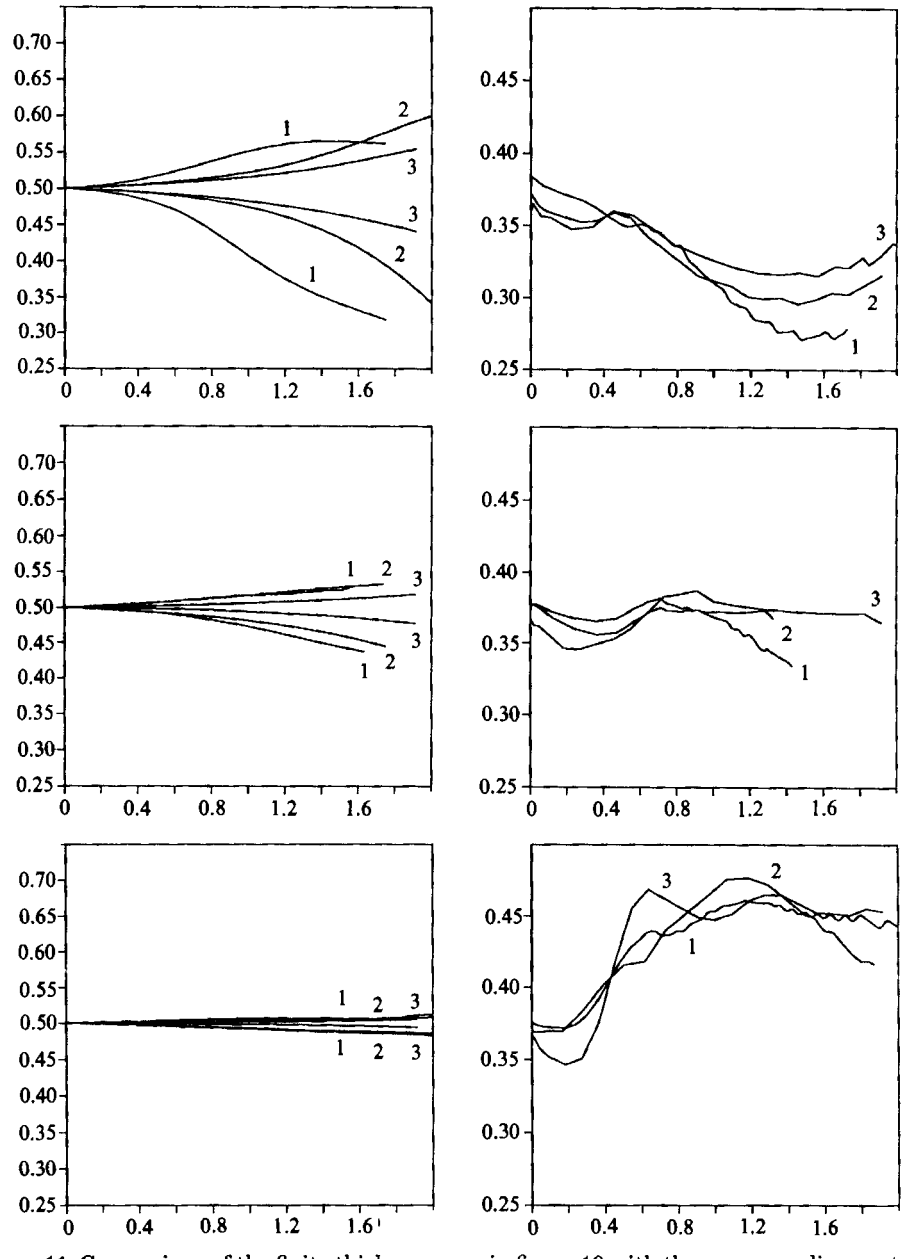

FIGURE 11. Comparison of the finite thickness runs in figure 10 with the corresponding vortex-sheet calculation. The left-hand column: the maximum and minimum free-surface elevations versus time. The right-hand column: the horizontal location of the maximum free-surface depth versus time. 1 indicates the corresponding vortex sheet run, 2 the thinner vortex layer, and 3 the thicker one.

not. The vortex sheet evolves far into the nonlinear region, and analysis for the linear stage of the roll-up would cover only a very short time interval with respect to the surface evolution. Motivated by the observation that the roll-up is initially associated with a strong advection of vorticity toward the vortex centre, but once the vortex forms, the vortex undergoes only moderate changes, we have studied the

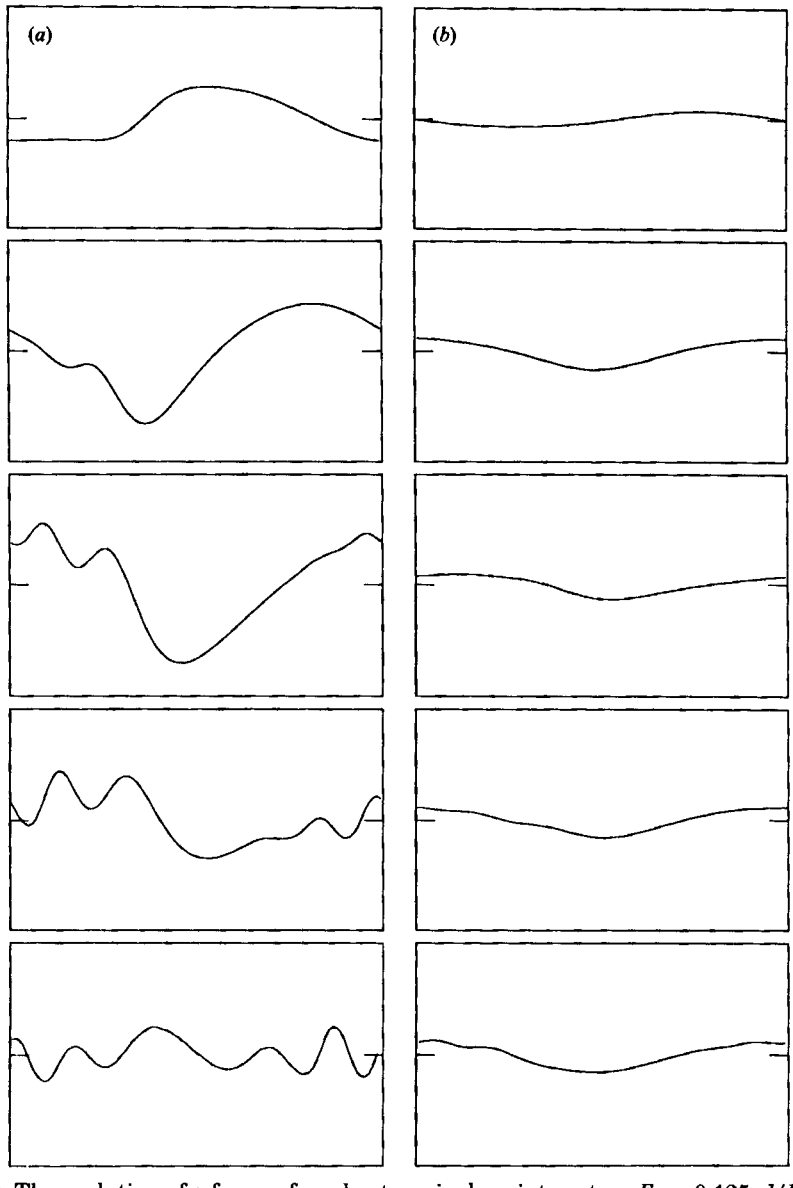

FIGURE 12. The evolution of a free surface due to a single point vortex; $Fr = 0.125$, $d/L = 0.4$. The non-dimensional times are approximately 0.5, 1.0, 1.5, 2.0 and 2.5. Profile (*a*): $\Gamma = \Gamma_0$. Profile (*b*): $\Gamma = \Gamma_0(1-e^{-1.5t})$. The amplitude is magnified 20 times.

surface disturbances of a vortex that is started impulsively for several depths and Froude numbers. As expected, the general surface signature is similar to the one generated by the shear layer, and the trend when the parameters are changed is the same. However, the quantitative agreement with the shear-layer calculations is generally not good. The main reason is that in the transition zone, where the inertial forces due to the vortical flow and the force of gravity are comparable, the detailed nature of the generation of a relatively concentrated vortex may be of considerable importance for the surface signature. To demonstrate this effect, we present two point vortex calculations in figure 12. In the first calculation, we simply assume that

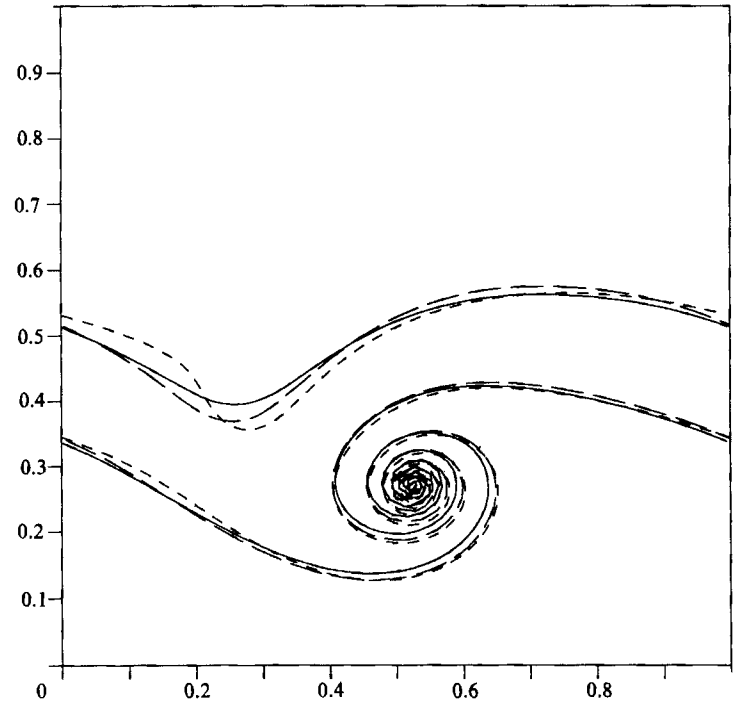

FIGURE 13. The effect of surface tension on the large-amplitude stage for $d/L = 0.2$ and $Fr = 1.0$ at non-dimensional time 1.25. ——, $We = 0.33$; — — —, $We = 1.0$; – – –, $We = \infty$.

the vortex is generated instantaneously, but in the second case the vortex forms gradually, mimicking the finite roll-up time. Here, $Fr = 0.125$, $d/L = 0.4$ and results are shown at times 0.5, 1.0, 1.5, 2.0 and 2.5. Since the surface motion is quite small, the amplitude is magnified 20 times, and only the free surface itself is shown. For the instantaneously generated vortex (figure 12*a*), short waves are generated, but for the vortex that starts gradually (figure 12*b*), only a single small depression forms. (The vortex has reached 0.9 times its final strength in the third frame.) The exact nature of the transient formation of a concentrated vortex from a shear layer may therefore, in general, have significant influence on the free-surface signature. Indeed, this is also the conclusion from our simulations of finite thickness shear layers in figure 10. We also mention that we have compared our point vortex calculations with linear predictions calculated by Hong (1988), and generally, we find good agreement under those conditions where agreement can be expected. These comparisons are presented in Yu (1990).

As in the previous section, we have investigated the effect of surface tension on a single case. In figure 13, the large-amplitude solution at time 1.25 is shown for $Fr = 1$ and $d/L = 0.2$, corresponding to one of the runs in figure 8. The solid line indicates $We = 0.33$, the long dashed line is for $We = 1.0$, and the dashed line is the infinite-Weber-number solution from figure 8. The major effect of surface tension is that it reduces the surface deformation in the region of highest curvature.

We end this section with simulations of more complicated situations: the pairing of vortices under a free surface and the collision of a vortex pair generated by a vortex sheet initially inclined with respect to the free surface. In figure 14, $Fr = 1.0$ and $d/L = 0.3$. The regularization parameter has been taken relatively large ($\delta = 0.2$)

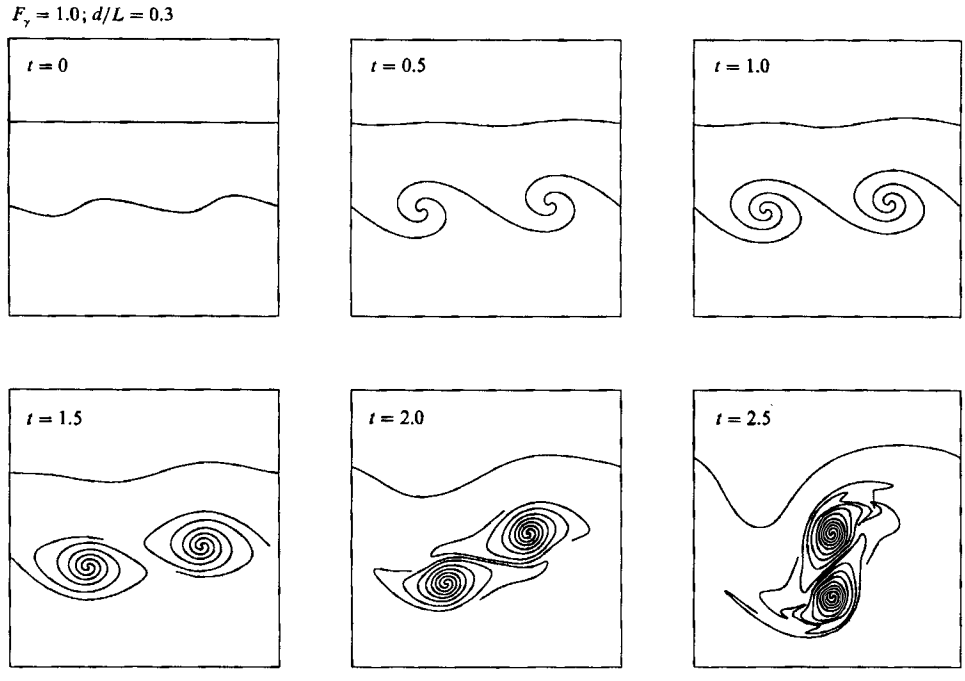

FIGURE 14. The surface signature of vortex pairing; $Fr = 1.0$, and $d/L = 0.3$.

to limit the number of computational elements needed to represent the inner part of the vortices. The vortex sheet is initially perturbed by two sine waves, one with a wavelength equal to the period length, and the other half as long and with three times the amplitude of the longer wave. First, the vortex sheet rolls up into two distinct vortices, and the surface deformation is similar to that predicted for a single wave in half the domain ($Fr = \sqrt{2}$ and $d/L = 0.6$). Then the vortices pair and drastically change the surface signature, making it more like that predicted for a single vortex at the same parameters. We have run similar cases, and generally we find that (i) for shallow vortices the pairing process quickly leads to high curvature that inhibits further simulations, and (ii) for deeper vortices the surface deformation is generally dominated by the pairing process. The experimental significance of this example is that in the absence of significant three-dimensional disturbances a weak shear layer might only produce large surface deformations after one or more vortex pairings have taken place.

Figure 15 shows a collision of a vortex pair with a free surface when the vortices approach the surface at an angle; the main surface deformation is due to the vortex that first encounters the surface. As the first vortex interacts with the surface, the other continues to propagate, causing the line connecting the vortices to become more aligned with the surface. The resulting deformation is similar to that of a single vortex interacting with the surface and will not be discussed in detail. In these particular calculations, the surface deformation leads to a breaking wave and the calculation could not be continued. We expect that at a later stage, both vortices will align with the surface, and the subsequent development will be more like the head-on collision problem.

For most of the simulations discussed in this report, we have monitored several additional parameters, such as the surface slopes, surface velocities, and upwelling of

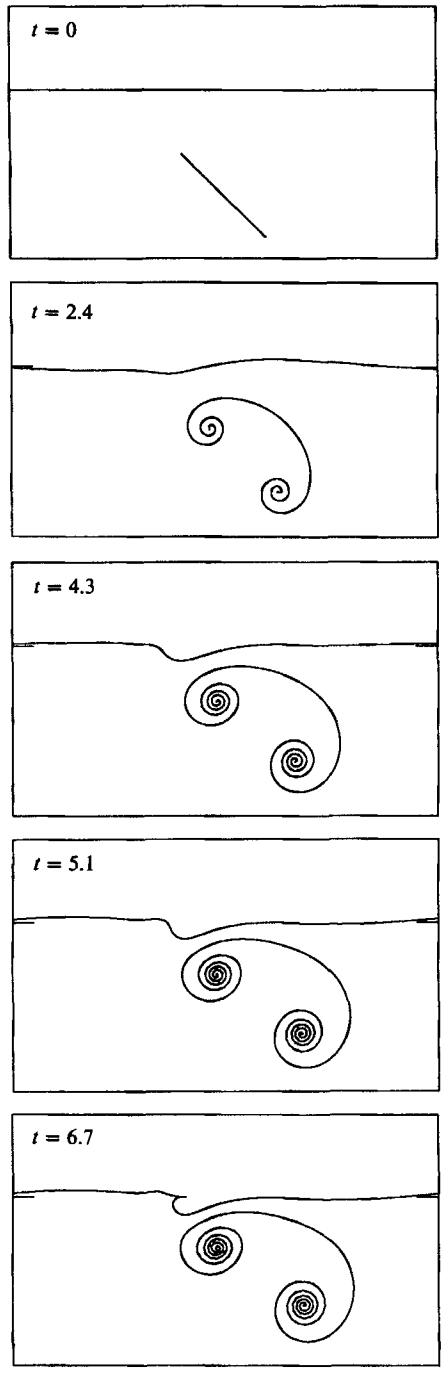

FIGURE 15. The evolution of a free surface owing to a collision of a vortex pair with an angle of 45°; average $d/L = 0.88$, $Fr = 3.54$.

fluids with the vortex pairs, which might be of interest in detailed comparisons with experimental data. Generally, we find that while such data provides some additional insight into the problem, the qualitative trend is obvious from the solution plots and the data we have presented. Thus, we will postpone the presentation of these diagnostics until experimental data is available for comparison. Preliminary comparisons in the case of a head-on collision of a vortex pair with a free surface appear in Willmarth *et al.* (1989).

4. Conclusions

For remote sensing, which provides the motivation for this study, the most important question is, how much can we tell about the submerged vortical flow from observations of the free surface? Though it is likely that a complete solution to this inverse problem does not exist, the Froude number obviously has a great influence on the free-surface deformation due to vortex motion. In the vortex collison problem, the Froude number is the main controlling parameter, and the geometric parameters such as the initial relative depth and the core size appear to play minor roles (at least for the cases that we investigated). For the shear-layer problem, there was an additional controlling parameter, the relative depth. This parameter could have been eliminated by considering an infinitely long domain; indeed, for the relatively shallow flows, the boundaries of the domain do not seem to influence the evolution significantly, except for the largest Froude numbers. Generally, it appears that the interaction can be classified either as a high- or a low-Froude-number motion. In the low-Froude-number case, the vortices interact with the surface as if it were a rigid wall. The surface deformations are relatively small, and their amplitude diminishes with decreasing Froude number. For transient motion in this limit, waves of wavelength different from the lengthscales of the vortical flows are sometimes generated. In the high-Froude-number limit, the vortices are sufficiently strong that they push the free surface around as if it were simply a passive marker. However, the result is a large surface deformation that eventually causes the surface motion to differ from what a passive interface would do. In this limit, the surface motion is directly related to the vortical flow, but, at least initially, is only weakly dependent on the Froude number. Hence, given a shapshot of the free surface at a fixed time, and some minimal information about the vortex configuration, the corresponding Froude number can only be determined in the low-Froude-number limit (refer to figure 3).

Physical intuition suggests that eventually some Froude number dependence will appear in the high-Froude-number limit, and this is what is observed for the shear-layer case but the calculations for the vortex pair collision could not be continued sufficiently far to establish what would happen eventually. For the vortex pair, it is likely that the scenario similar to the one observed by Dahm *et al.* (1989) for vortex collision with weakly stratified density interfaces takes place. The fluid accompanying the vortex pair is gradually 'stripped' away, and for the finite area vortex regions and the vortex sheet, the vortical fluid itself is eventually 'thrown' back by the ever increasing reaction from the surface. One may also speculate that in some cases the fluid blob will fall outward, as suggested by figure 2. In the case of the point vortices, however, such 'stripping' cannot reduce the vorticity of the fluid, and indeed it seems more likely that the long-time behaviour is given by a point vortex pair pushed closer and closer, and moving faster and faster with less and less fluid,

possibly resulting in a singularity. The present calculations have not been able to answer this question, and we may note that for a real fluid the vortices always have a finite core and that viscosity presumably will greatly affect the long-time behaviour.

While the transitional region, when the inertial forces due to the vortical motion and gravity are of roughly the same magnitude (note that this happens for a Froude number of the order unity), is in some sense the most interesting, the limits may have equally practical significance from an observational point of view. For example, a 'white water' region of splashes indicate strong vortices with lengthscales comparable to the disturbances, but gentle, wavy flow indicates weaker vortices where a one-to-one correspondence may not exist between the disturbance lengthscale and those of the vortical flow. Previous calculations of point vortex collision with a free surface have been limited to a few Froude numbers around the transition value and thus did not address what would happen for smaller or larger values of the Froude number. Furthermore, by considering only a single initial condition (two point vortices), no generalizations could be made.

This study is our first step in an effort to develop a comprehensive understanding of the free-surface signature of submerged, unsteady vortical flows. The flows considered are therefore relatively simple, and we conclude with a few remarks about the limitations of this present study. The most restrictive assumption, presumably, is that we have confined our attention to two-dimensional models. While such models are relevant to certain experimental situations and produce considerable insight into some of the interaction mechanisms, most of the vortex interactions observed experimentally involve fully three-dimensional motions. In the experiments of Sarpkaya (1986) and Hirsa (1990) on the surface signature of trailing vortices, for example, the appearance of striations is a three-dimensional phenomena. Also, in Bernal's experiments with subsurface jets (Bernal & Madnia 1989) and vortex rings (Bernal & Kwon 1989), the predominant wave-making mechanism is the 'opening up' of vortex rings colliding obliquely with the surface. These fully three-dimensional aspects are naturally outside the scope of our two-dimensional models.

Another complication is the presence of surface contaminants on real free surfaces. Generally, the surface motion created by vortical flow results in an uneven distribution of the contaminants and thus non-uniform surface tension. While the effect of surface contaminants on the damping of surface waves is reasonably well understood, the effects on vortical structures below the free surface have received much less attention. Barker & Crow (1977) observed that a vortex pair colliding with the surface produces secondary vortices and rebounds, as when vortices collide with a rigid surface. Saffman (1979) pointed out that for inviscid flow and a flat boundary, rebounding cannot occur and suggested that the behaviour might be due to surface tension effects. On the basis of numerical simulations, Peace & Riley (1983) argued that even for stress-free boundaries, viscosity would cause rebounding. However, their calculations were for rather low Reynolds numbers, and with an increasing Reynolds number, the rebounding decreased significantly.

Recent experimental studies by Bernal *et al.* (1989) have demonstrated a rather dramatic dependence on the cleanness of the surface. For a clean surface, the vortical motion behaves as would be expected from an inviscid analysis (if the surface deforms, some rebounding is predicted, but most of the experiments have been performed under conditions where surface deformation is minimal). But in the presence of surface contamination, the shear stress induced by uneven surface tension results in considerable vorticity production and subsequent boundary-layer

separation, whereby this vorticity is swept into the interior. This injection of vorticity and its subsequent interaction with the primary vorticity appears to be the leading effect of the surface contaminants. While our inviscid method is easily modified to account for constant surface tension (figures 6 and 13) and can easily predict the redistribution of a surface contaminant, the resulting shear stress is incompatible with the inviscid model.

This work was supported by the Program in Ship Hydrodynamics (PSH) at The University of Michigan, funded by the University Research Initiative of the Office of Naval Research (contract no. N000184-86-K-0684), and by National Science Foundation grant MSM-8707646. Constructive interaction with Professors W. W. Willmarth, W. J. A. Dahm, L. Bernal, and other members of the PSH has been most helpful in carrying out the research discussed here. The calculations were done mostly on the computers at the San Diego Supercomputer Center, which is sponsored by the NSF.

REFERENCES

BAKER, G. R., MEIRON, D. I. & ORSZAG, S. A. 1982 Generalized vortex methods for free surface flow problem. *J. Fluid Mech.* **123**, 477–501.

BARKER, S. J. & CROW, S. C. 1977 The motion of two-dimensional vortex pairs in a ground effect. *J. Fluid Mech.* **82**, 659–671.

BERNAL, L. P., HIRSA, A., KWON, J. T. & WILLMARTH, W. W. 1989 On the interaction of vortex rings and pairs with a free surface for various amounts of a surface active agent. *Phys. Fluids* A **4**, 2001–2004.

BERNAL, L. P. & KWON, J. T. 1989 Vortex ring dynamics at a free surface. *Phys. Fluids* A **1**, 449–451.

BERNAL, L. P. & MADNIA, K. 1989 Interaction of a turbulent round jet with the free surface. In *Proc. 17th Symp. on Naval Hydrodynamics*, pp. 79–87. National Academy Press.

CAFLISCH, R. E. & LOWENGRUB, J. S. 1989 Convergence of the vortex method for vortex sheets. *SIAM J. Numer. Anal.* **26**, 1060–1080.

DAGAN, G. & TULIN, M. P. 1972 Two-dimensional free surface gravity flow past blunt bodies. *J. Fluid Mech.* **51**, 529–543.

DAHM, W. J. A., SCHEIL, C. M. & TRYGGVASON, G. 1989 Dynamics of vortex interaction with a density interface. *J. Fluid Mech.* **205**, 1–43.

DAVIES, J. T. 1966 The effects of surface films in damping eddies at a free surface of a turbulent liquid. *Proc. R. Phys. Soc.* A **290**, 515–526.

DAVIES, J. T. & DRISCOLL, J. P. 1974 Eddies at free surfaces, simulated by pulses of water. *Ind. Engng Chem., Fundam.* **13**, 105–109.

DOLD, J. W. & PEREGRINE, D. H. 1986 An efficient boundary-integral method for steep unsteady water waves. In *Numerical Methods for Fluid Dynamics*, vol. 2, (ed. K. W. Morton & M. J. Bains), pp. 671–679. Oxford University Press.

HIRSA, A. 1990 An experimental investigation of vortex pair interaction with a clean or contaminated free surface. Ph.D. thesis, The University of Michigan.

HONG, W. W. 1988 Unsteady separated flow around a two-dimensional bluff body near a free surface. PhD thesis, The University of Michigan.

KOCHIN, N. E., KIBEL, I. A. & ROZE, N. V. 1964 *Theoretical Hydrodynamics*. Interscience.

KRASNY, R. 1986 Desingularization of periodic vortex sheet roll up. *J. Comp. Phys.* **65**, 292–313.

KRASNY, R. 1988 Computation of vortex sheet roll-up in the Trefftz plane. *J. Fluid Mech.* **184**, 123–155.

LEONARD, A. 1980 Vortex methods for flow simulation. *J. Comp. Phys.* **37**, 289–335.

LONGUET-HIGGINS, M. S. & COKELET, E. D. 1976 The deformation of steep surface waves on water. II. Growth of normal-mode instabilities. *Proc. R. Soc. Lond.* A **364**, 1–28.

LUGT, H. J. 1981 Numerical modelling of vortex flows in ship hydrodynamics. *Third Intl Conf. on Numerical Ship Hydrodynamics*, pp. 297–317 (ed. J. C. Dern & H. J. Hausslineg).

LUGT, H. J. 1983 *Vortex Flow in Nature and Technology*. Wiley.

MARCUS, D. L. 1988 The interaction between a pair of counter-rotating vortices and a free boundary. PhD thesis. The University of California at Berkeley.

NOVIKOV, YE. A. 1981 Generation of surface waves by discrete vortices. *Izv. Atmospheric and Oceanic Physics* **17**, 709–714.

PEACE, A. J. & RILEY, N. 1983 A viscous vortex pair in ground effect. *J. Fluid Mech.* **129**, 409–426.

POZRIKIDIS, C. & HIGDON, J. J. L. 1985 Nonlinear Kelvin–Helmholtz instability of a finite vortex layer. *J. Fluid Mech.* **157**, 225–263.

SAFFMAN, P. G. 1979 The approach of a vortex pair to a plane surface in inviscid fluid. *J. Fluid Mech.* **92**, 497–503.

SALVESEN, N. & KERCZEK, C. VON 1976 Comparison of numerical and perturbation solutions of two-dimensional nonlinear water-wave problems. *J. Ship Research* **20**, 160–170.

SARPKAYA, T. 1986 Trailing-vortex wakes on the free surface. *16th Symp. on Naval Hydrodyn.* pp. 38–50. National Academy Press.

SARPKAYA, T. 1989 Computational methods with vortices – the 1988 Freeman scholar lecture. *Trans. ASME* I: *J. Fluids Engng* **111**, 5–52.

SARPKAYA, T., ELNITSKY, J. & LEEKER, R. E. 1989 Wake of a vortex pair on the free surface. *Seventeenth Symp. on Naval Hydrodyn.* pp. 53–60. National Academy Press.

SAUNDERS, H. E. 1965 *Hydrodynamics in Ship Design*, vol. 3. SNAME.

SCHULTZ, W. W. 1987 A complex-valued integral method for free surfaces with intersecting bodies. In *Second International Workshop on Water Waves and Floating Bodies, Bristol, England* (ed. D. Evans), pp. 101–104.

SHAMPINE, L. F. & GORDON, M. K. 1965 *Computer Solution of Ordinary Differential Equations*. Freeman.

SONG, M., YU, D. & TRYGGVASON, G. 1988 Vortex interaction with a free surface. *Bull. Am. Phys. Soc.* **33**, 2279 (abstract only).

TELSTE, J. H. 1989 Potential flow about two counter-rotating vortices approaching a free surface. *J. Fluid Mech.* **201**, 259–278.

TRYGGVASON, G. 1988 Deformation of a free surface as a result of vortical flows. *Phys. Fluids* **31**, 955–957.

TRYGGVASON, G. 1989 Vortex dynamics of stratified flows. *Mathematical Aspects of Vortex Dynamics* (ed. R. E. Caflisch), pp. 160–170. SIAM.

VINJE, T. & BREVIG, P. 1981 Numerical simulation of breaking waves. *Adv. Water Resources* **4**, 77–82.

WEHAUSEN, J. V. & LAITONE, E. V. 1960 Surface waves. *Encyclopedia of Physics*, vol. 9, pp. 446–778. Springer.

WILLMARTH, W. W., TRYGGVASON, G., HIRSA, A. & YU, D. 1989 Vortex pair generation and interaction with a free surface. *Phys. Fluids* A **1**, 170–172.

YU, D. 1990 Numerical simulations of vortex interactions with a free surface PhD thesis. The University of Michigan.

ZABUSKY, N. Y., HUGHES, M. H. & ROBERTS, K. V. 1979 Contour dynamics for the Eular equations in two-dimensions. *J. Comp. Phys.* **30**, 96–106.